Investigation of Hydrological Variability in West Africa Using Land Surface Models

K. Y. LI,* M. T. COE, AND N. RAMANKUTTY

Center for Sustainability and the Global Environment, Gaylord Nelson Institute for Environmental Studies, University of Wisconsin—Madison, Madison, Wisconsin

ABSTRACT

The availability of freshwater is a particularly important issue in Africa where large portions of the continent are arid or semiarid and climate is highly variable. Sustainable water resource management requires the assessment of hydrological variability in response to nature climate fluctuation. In this study, a land surface model, the Integrated Biosphere Simulator (IBIS), and a hydrological routing model, the Hydrological Routing Algorithm (HYDRA), are used to investigate the hydrological variability in two large basins, the Lake Chad basin (LCB) and the Niger River basin (NRB), located in West Africa, over the period from 1950 to 1995. The IBIS land surface hydrological module was calibrated and validated for arid and semiarid Africa, and major enhancements were made to the module, including the development of a dynamic root water–extraction formulation, the incorporation of a Green–Ampt infiltration parameterization, and modification to the prescribed root distribution, the runoff module, and weather generator. The results show that the hydrology in this area is highly variable over time and space. The coefficient of variance (CV) of annual rainfall ranges from 10%–15% in the southern portions of the basins to 30%–40% in the northern portions. The annual evapotranspiration (ET) varies with a slightly lower CV compared to the rainfall, but the runoff is extremely sensitive to the rainfall fluctuation, particularly in the central portions of the basins (8°–13°N in LCB and 12°–16°N in NRB) where the CVs in runoff are as high as 100%–200%. The annual river discharge varies largely in concert with the rainfall fluctuation, with the CV being 37% in LCB and 23%–63% in NRB. In terms of the whole basin, the relative hydrologic variability (rainfall, evapotranspiration, runoff, and river discharge) is significantly higher in the dry period than in the wet period, and the interannual variability in runoff is more than twice as high as compared to rainfall or ET.

1. Introduction

The availability of freshwater is of growing concern to academics, policy makers, and the international community; human well-being, ecosystem health, and functioning, as well as economics and politics, all depend on how much, when, and where water is available (Gleick 2000). It is a particularly important issue in Africa where large portions of the continent are arid or semiarid and climate is highly variable (Ashton 2002). Climate variation has a profound impact on hydrology and

water resources. An understanding of how hydrologic cycles and water resources respond to climate variation is necessary for sustainable water resource management. This study focuses on addressing the hydrologic impacts of interannual climate variability in the Lake Chad and Niger River basins, located in West Africa, over the period from 1950 to 1995.

Hydrologic models provide a means of investigating the relationships between water cycles and climate, particularly where data are limiting (Leavesley 1994; Legesse et al. 2003). The current hydrologic modeling approaches can be broadly classified into four categories: empirical, water balance, conceptual, and physically based distributed models (Leavesley 1994; Legesse et al. 2003). The model choice depends on application objective, data availability, and spatial and temporal scales. Although empirical models have minimal data requirements and may produce good estimates within the range of their calibration data, they are questionable when applied to basins and climate conditions dif-

* Current affiliation: University of Washington Hydrology Group, University of Washington, Seattle, Washington.

Corresponding author address: Dr. K. Y. Li, University of Washington Hydrology Group, University of Washington, Box 352700, Seattle, WA 98195-2700.
E-mail: likaiyuan@gmail.com

ferent from those used to develop the models. They also provide few insights into the way hydrologic systems function. Water balance models are of monthly or annual time step, and therefore cannot simulate individual runoff events at time steps of hours or days. Conceptual models are developed using approximations or simplifications of fundamental physical laws with some amount of empiricism; they are more detailed and of higher temporal resolution, but more parameters and data are required as compared to the empirical and the water balance models. Physically based models are more appropriate for interpreting and predicting the impacts of climate variation/change and human activities. Land surface models are physically based and distributed models, which simulate not only hydrological processes, but also biophysical and biogeochemical processes of the soil–plant–atmosphere system. Therefore, it is often desirable to use them to investigate the interactions between hydrological, ecological, and atmospheric processes.

In this study we use two physically based models—a land surface model, the Integrated Biosphere Simulator (IBIS) (Foley et al. 1996; Kucharik et al. 2000), and a hydrological routing model, the Hydrological Routing Algorithm (HYDRA) (Coe 1998, 2000)—to simulate the hydrology of the Lake Chad and Niger River basins of West Africa. While IBIS has been widely tested globally and regionally (e.g., Kucharik et al. 2000; Delire and Foley 1999; Lenters et al. 2000), including in the Lake Chad basin (Coe and Foley 2001), the stand-alone hydrologic performance for arid and semiarid regions requires further evaluation. Therefore, the objectives of this study are twofold: 1) to enhance, calibrate, and validate the IBIS hydrological module for arid and semiarid Africa, and 2) to simulate the spatial and interannual variability of the regional hydrology for the period from 1950 to 1995.

2. Methodology

a. IBIS description

IBIS is designed to integrate a variety of terrestrial ecosystem phenomena within a single, physically consistent model (Foley et al. 1996). The model simulates a wide range of processes including land surface physics, canopy physiology, vegetation phenology, terrestrial carbon balance, and vegetation dynamics. Since the overall description of IBIS can be found in Foley et al. (1996) and Kucharik et al. (2000), only the land surface hydrological module is described below.

The hydrologic module, based on the land surface transfer scheme (LSX) (Thompson and Pollard 1995a,b), represents two vegetation canopies (i.e.,

woody and herbaceous plants), six soil layers, and three layers of snow.

1) SOIL MOISTURE

A six-layer soil moisture model, extending from the surface to a depth of 4 m, describes the diurnal and seasonal cycles of soil moisture. The dynamics of soil volumetric water content and ice content are simulated for each layer. The soil moisture simulation is based on the Richards equation expressed as

$$\frac{\partial \theta}{\partial t} = \frac{\partial}{\partial z}\left(D(\theta)\frac{\partial \theta}{\partial z}\right) + \frac{\partial K(\theta)}{\partial z} - \text{ST}(z, t), \quad (1)$$

where θ is volumetric soil moisture content; t the time; D a diffusion coefficient; K the hydraulic conductivity; z the vertical coordinate, positive upward; and ST a sink term, which represents water uptake by plant roots.

The sink term (ST) is a function of plant transpiration (P), which is calculated as described below based on Pollard and Thompson (1995):

$$E_u = \frac{\rho s_u}{(1 + r_u s_u)}(1 - f_u^{\text{wet}})(q_{\text{sat}}(T_u) - q_{12})\,\text{LAI}_u, \quad (2)$$

$$E_l = \frac{\rho s_l}{(1 + r_l s_l)}(1 - f_l^{\text{wet}})(q_{\text{sat}}(T_l) - q_{34})\,\text{LAI}_l, \quad (3)$$

$$P = E_u + E_l, \quad (4)$$

where the subscripts u and l denote *upper*-story leaves and *lower*-story leaves; E_u and E_l are transpiration fluxes from unit leaf area to air (kg m^{-2} s^{-1}); ρ is the density of near-surface air (kg m^{-3}); f_u^{wet} and f_l^{wet} represent the fraction of leaf area wetted by intercepted liquid or snow; T_u and T_l are leaf temperature (K); s_u and s_l are a heat/vapor transfer coefficient between vegetation and canopy air (m s^{-1}); r_u and r_l denote stomatal resistance per unit leaf area for the upper and lower story (s m^{-1}); $q_{\text{sat}}(T)$ is saturation specific humidity versus temperature at ambient pressure (kg kg^{-1}); q_{12} and q_{34} are repsectively upper and lower canopy air specific humidity (kg kg^{-1}); LAI$_u$ and LAI$_l$ are upper and lower canopy leaf area index (single sided, m^2 m^{-2}).

2) ROOT WATER UPTAKE

Modeling soil water flow including vegetation requires a description of water uptake by plant roots to calculate the sink term ST in Eq. (1). In IBIS, the water uptake by plant roots for a given soil layer i, is described as

$$S_i = PF_i, \quad (5)$$

where S (m s^{-1}) is water uptake in the soil layer i, P is plant transpiration (m s^{-1}), and F is water uptake fraction, a function of both root distribution and soil water availability. If the soil profile within the root zone is divided into n layers, then the water uptake fraction (F) for a given layer i, is defined as

$$F_i = \frac{R_i W_i}{\sum\limits_{j=1}^{n} R_j W_j}, \qquad (6)$$

where R is root biomass fraction and W is soil water availability factor, defined as

$$W = \frac{1.0 - \exp(e\theta_a)}{1.0 - \exp(e)}, \qquad (7)$$

where e is a stress factor that determines the strength of the soil moisture stress on physiological process ($e = -5.0$ in the current version of IBIS), and θ_a is the available water fraction, expressed as

$$\theta_a = \frac{\theta - \theta_w}{\theta_f - \theta_w}, \qquad (8)$$

where θ is actual soil water content (m^3 m^{-3}), θ_w the wilting point (m^3 m^{-3}), and θ_f the field capacity (m^3 m^{-3}).

The root biomass fraction R is calculated as

$$R_i = Y_i - Y_{i-1}, \qquad (9)$$

where Y is the cumulative root fraction from surface to the corresponding soil layer, represented by an asymptotic equation (Gale and Grigal 1987),

$$Y = 1 - \beta^d, \qquad (10)$$

in which d is soil depth (cm) and β is a simple numerical index that determines root distribution with depth. High β values (e.g., 0.99) are associated with a larger proportion of roots at deeper soil depth relative to low values of β (e.g., 0.90), which implies a larger proportion of roots near the soil surface. Jackson et al. (1996, 1997) compiled a database of global root studies and provided β values for various biomes.

Total water stress (denoted as α), an important parameter that largely controls stomatal resistance and hence the transpiration rate P, is represented as

$$\alpha = \sum_{i=1}^{n} R_i W_i. \qquad (11)$$

3) INFILTRATION AND RUNOFF

Infiltration is estimated based on Darcy's law (Pollard and Thompson 1995). Surface runoff occurs when the surface puddle exceeds the maximum puddle depth, which is a lumped parameter rather than a distributed parameter, and is determined primarily by climate and vegetation type, soil texture, and topography. Since the maximum puddle depth is a constant over space and time, the surface runoff module, in this form, is unable to handle the local and ephemeral ponds (also termed endorheic basins, because they have no outflow other than through evaporation). Consequently, we have made a significant enhancement to this surface runoff module such that, as described later in the model enhancement section, it is capable of dealing with endorheic hydrological issues. Free drainage is allowed in the soil water calculation, and the total runoff is the sum of the surface runoff and the subsurface drainage.

4) WEATHER GENERATOR

Daily or hourly weather data are normally required by physically based land surface models. However, these data are not readily available in many regions, especially for long historical records. IBIS generates daily and hourly weather from monthly weather data using a stochastic weather generator as developed by Richardson and Wright (1984), Richardson (1981), and Geng et al. (1985). The hourly data are generated from daily data. Hourly air temperature and humidity are estimated using a method developed by Campbell and Norman (1998). Hourly wind speed is calculated following an equation from the Environmental Policy Integrated Climate (EPIC) weather generator (Williams 1995). The starting and ending time and duration of a rainfall or snow event are randomly generated within each day.

b. HYDRA description

HYDRA simulates the time-varying flow and storage of water in terrestrial hydrological systems, including rivers, inundated floodplains, and lakes. The model operates on a 5-min latitude by longitude grid (~9 km at the equator) with a 1-h time step. The model is based on a linear reservoir model and simulates the stage and discharge of rivers and the stage and geographic extent of inundated floodplains and lakes in terms of river-routing directions derived from local morphology, residence times within a grid cell, and effective flow velocities. Within the hydrologic network, the total water influent to each grid cell is the sum of the land surface runoff (R_s), subsurface runoff (R_d), precipitation (P_w), evaporation (E_w) from the surface waters, and the water flow from upstream grid cells (m^3 s^{-1}). The water transport is represented by the time-dependent change of three water reservoirs (m^3): river water reservoir (W_r), surface runoff pool (W_s), and subsurface drainage

pool (W_d). The W_r contains the sum of upstream and local water in excess of that required to fill a local surface water depression. The W_s represents the water that has run off the surface locally, while the W_d stands for the water that has drained through the local soil column, both flowing toward a river. The change with time of these three reservoirs is governed by the following differential equations:

$$d(W_s)/dt = R_s - W_s/T_s \; d(W_d)/dt \tag{12a}$$
$$= R_d - W_d/T_d \; d(w_r)/dt \tag{12b}$$
$$= (W_s/T_s + W_d/T_d) \times (1 - A_w) + (P_w - E_w)$$
$$\times A_w - (W_r/T_r) + F_{in}, \tag{12c}$$

where A_w is the predicted fractional water area in the grid cell, ranging from 0 (no water present) to 1 (the grid cell completely covered by a lake or wetland); T_s, T_d, and T_r are the residence times (s) of the water in each of the reservoirs; P_w and E_w are the precipitation and evaporation rates ($m^3 \, s^{-1}$) over the surface water, respectively; and ΣF_{in} is the sum of the water fluxes ($m^3 \, s^{-1}$) from the upstream cells. For details of the model, readers are referred to Coe (1998, 2000) and Coe et al. (2002). The version of HYDRA used in this study differs from that described in Coe et al. (2002) in that the river directions are not prescribed but are calculated dynamically at each time step based on the water head (land elevation plus the water depth). This change allows for a more dynamic simulation of instream wetlands on the Niger and Lake Chad river systems.

c. Brief description of the simulated basins

The Lake Chad basin (LCB) (Fig. 1), located in West Africa, extends over seven countries. The most important rivers influent into the lake are the Chari and its tributary the Logone, the Komadougou-Yobe, the El Beid, and the Yedseram. The mean annual rainfall varies from 1500 mm in the southern parts to less than 100 mm in the northern parts, with an average over our simulated domain of 373 mm. The Niger River basin (NRB) (Fig. 1), the second largest basin shared by 11 countries in Africa, is situated to the west of LCB. The mean annual rainfall over our simulated domain is 425 mm ranging from 20 to 650 mm in the northern parts and from 1000 to more than 1500 mm in the southern parts of the basin. Both basins straddle the boundary between the Sahara Desert and the moist tropical forest to the south and are characterized by high precipitation variability over the long and short term (Nicholson 1988, 2000). In both basins, vegetation is dominated by tropical forests and savanna/grassland in the southern
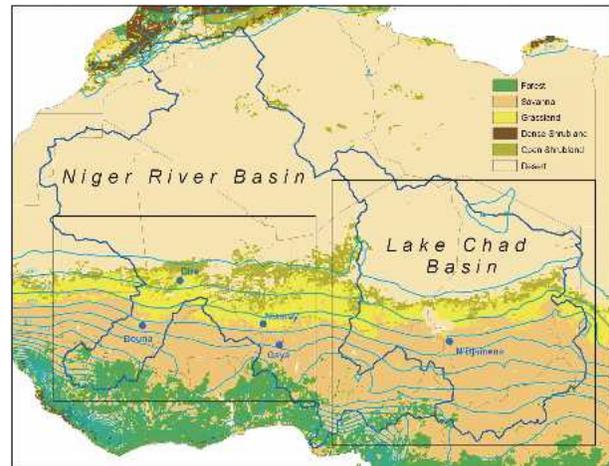

FIG. 1. Lake Chad basin (LCB) and Niger River basin (NRB) with potential vegetation types and isohyets (mm yr^{-1}).

portion with very little vegetation in the northern portion (Fig. 1). Generally, the climate for both basins was relatively wet before the late 1960s and has been relatively dry ever since (Fig. 2).

The potential drainage basin areas for the Lake Chad and Niger River basins are defined from the 5′ resolution digital elevation model (DEM) used in HYDRA (Fig. 1). Much of the basin areas in the north do not contribute runoff to the river systems in the present climate. Therefore, the domains (denoted by the boxes in the Fig. 1) over which we simulate the water balances in this study are smaller than the potential basin areas. The simulation domains were chosen so that all land
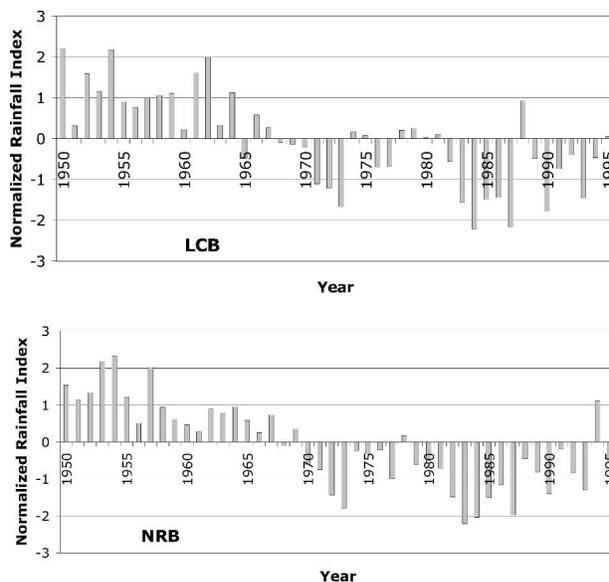

FIG. 2. Rainfall index of the LCB and NRB in 1950–95.

surface area contributing runoff upstream of our gauge data is included. The simulated basin area of the LCB is 2.40×10^6 km^2, similar to that reported in the literature. The simulated area of the NRB is 1.83×10^6 km^2. The simulated NRB area differs from the area cited in literature (2.1×10^6 km^2) because we do not include most of the basin area downstream of Gaya and other sources do not include the large area in the Sahara as part of the NRB. All of our discussions below are based on the simulated basin areas.

d. Experiment design

For these experiments IBIS was run at the resolution of $0.5° \times 0.5°$ and a time step of 1 h. The model input data include monthly mean climate data for the period 1937–95 (New et al. 2000), potential natural vegetation type derived from Ramankutty and Foley (1999), and soil type from the International Geosphere-Biosphere Programme–Data and Information System [IGBP–DIS (1999)] as used by Coe and Foley (2001). The vegetation types were fixed in the simulations to the potential natural classes, and therefore historical land-use/cover changes are not considered in this study. We should include a caveat here that we likely underestimate forest cover in the southern portions of the basins because the methodology used by Ramankutty and Foley (1999) used remotely sensed depictions of land cover in areas that were not identified by the satellite as human modified; it is likely that the savannas in West Africa that are identified as potential natural vegetation here are a product of several millennia of human use. The output calculated by IBIS includes surface runoff, drainage, evapotranspiration, and soil moisture content. The surface runoff and drainage produced by the IBIS was then routed to the basin outlets using HYDRA at the resolution of $5' \times 5'$ and with 1-h time step.

3. Model enhancement

Initial simulations indicated that IBIS significantly overestimated both surface runoff and drainage in arid and semiarid Africa (data not shown). After many sensitivity simulations aimed at identifying the major factors influencing hydrologic performance, we found that the runoff overestimation in Africa could be attributed to the following factors within IBIS: 1) relatively shallow rooting depth and low water uptake at deep soil layers, a major factor responsible for the overestimation of drainage; 2) low infiltration rates, contributing to the overestimation of the surface runoff; and 3) unrealistically large rainfall events created by the weather generator. Additionally, the partitioning of the rainfall between soil infiltration and surface runoff is largely controlled by the empirical maximum puddle depth parameter as previously described. In the original version of IBIS, the maximum puddle depth is a lumped parameter, meaning that a constant empirical value is used in the whole basin over the whole period; however, a spatially and temporally varying parameter would be more accurate. Given these limitations, the following major enhancements were made to the IBIS hydrological module.

a. Rooting depth and root distribution

Root distribution varies with biomes, soil types, and climate conditions and is usually difficult to represent in land surface models. Equation (10) is the vertical root distribution function used in IBIS, where β is the only parameter that controls the root distribution pattern. The advantage of Eq. (10) is that only one parameter (β) is required. The β values for various biomes were estimated from the worldwide measurements (Jackson et al. 1996, 1997). However, since almost all of this root distribution data were collected in the top 2 m of soil, the maximum rooting depth in the IBIS is roughly 2 m and the β values used are, therefore, most likely biased. A study by Canadell et al. (1996) reports that the maximum rooting depth by biome ranges from 2.0 ± 0.3 m for boreal forest to 15.0 ± 5.4 m for tropical grassland/savanna, with a global average of 4.6 ± 0.5 m. Usually, the rooting depth in a dry climate is deeper than in a wet one. Therefore, 2 m is not sufficiently deep in arid and semiarid Africa. Here we assume that in arid and semiarid Africa 5% of the root biomass for trees and 2% for herbaceous plants are distributed below 2 m. Based on this assumption, we reestimated the β values: $\beta = 0.9806$ for lower canopy herbaceous plants and $\beta = 0.9851$ for upper canopy trees.

The root distribution and rooting depth has significant effect on the total runoff. The simulated total runoff with the modified root distribution is significantly lower than the one with the original IBIS root distribution (Fig. 3). This is because the modified root distribution increases the water extraction in the deep soil layers (below 2 m) and hence greatly reduces the drainage. Because the observed drainage is very limited in arid and semiarid Africa, the simulation with the modified root distribution appears to be more realistic.

b. Root water extraction

While a small fraction of root biomass exists at the depth below 2 m, these roots may be relatively more
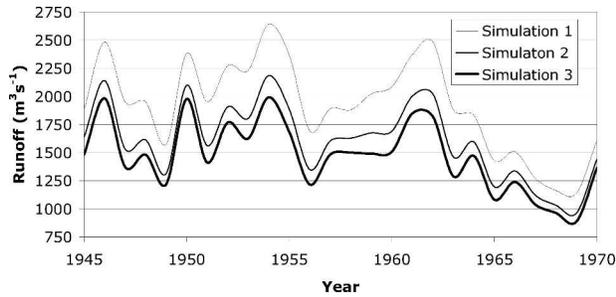
FIG. 3. Model sensitivity to root water–uptake functions and root distribution patterns in the LCB: simulation 1: original root water–uptake function and original β values; simulation 2: original root water–uptake function and modified β values; and simulation 3: new dynamic root water–uptake function and modified β values.

FIG. 4. Water-uptake patterns with different λ values under optimum soil moisture condition (the depth of the soil compartment is 10 cm).

important than those in shallow layers under arid and semiarid climate conditions. The water uptake by plants during the wet season comes from shallow layers; however, as those layers become dry, there is a progressive shift toward using deeper water (see the reviews by Gardner 1983 and by Canadell et al. 1996). This implies that the water stress occurring in the densely rooted shallow layers can be compensated through increasing the water extraction from sparsely rooted, wetter, deeper layers. Apparently, the relative importance of the roots varies with depth and soil moisture distribution profile.

The original IBIS root water–uptake module does not adequately consider the relative functional importance of the roots and water stress compensation. In this study, the original module is modified to allow dynamic allocation of root water uptake. This new formulation dynamically adjusts the relative importance of the roots in water uptake according to the soil moisture profile, thereby allowing the water stress occurring in one dry layer to be compensated by increasing water uptake from other wetter layers. The idea of this dynamic model is similar to a crop root water–uptake model developed by Li et al. (2001), but a dynamic, instead of static, exponent λ is introduced to the root fraction R of Eq. (6). The water-uptake fraction (F) for a given layer i, is therefore redefined as

$$F_i = \frac{R_i^\lambda W_i}{\sum_{j=1}^{n} R_j^\lambda W_j}. \tag{13}$$

The exponent λ, which in part controls the relative importance of the roots in water uptake at each layer, varies with the vertical soil moisture distribution. Lower λ values (smaller than 1; e.g., 0.50) correspond
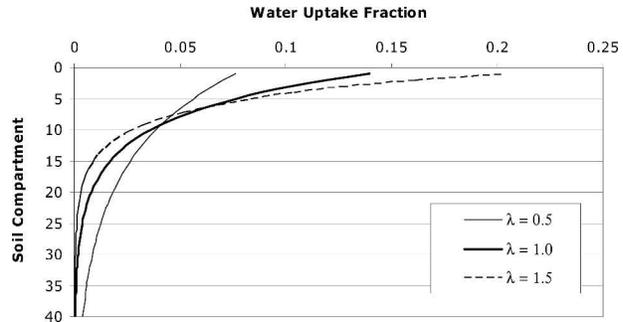
to a relatively larger proportion of water uptake at deep layers relative to higher λ values (larger than 1; e.g., 1.5), which is associated with a relatively greater proportion of water uptake at shallow depth (Fig. 4). In this study, a set of λ values (Table 1) is recommended according to the soil moisture profile pattern for the upper one-third and the lower two-thirds of the rooted zone. These recommended λ values are within the range of the reported values, including 0.5 (Li et al. 2001; Ehlers et al. 1991; Cooper et al. 1987; Bennie 1986), 1.0 (Hsiao et al. 1976; Taylor and Klepper 1975), 1.5 (De Smedt et al. 1981; van der Ploeg et al. 1978), and 2.0 (Passioura 1985). Through dynamically changing the λ value, the predominant water uptake moves downward in the dry season and upward in the wet season. In the Hydrological Atmospheric Pilot Experiment (HAPEX-Sahel), a similar concept was used to estimate the available water content to each plant by integrating the root distribution profile with the soil moisture profile (Hanan and Prince 1997)

Accordingly, the total water stress α, which partly determines stomatal resistance and thus plant transpiration, is redefined as follows:

$$\alpha = \sum_{i=1}^{n} F_i U_i, \tag{14}$$

TABLE 1. Dynamic exponent (λ) values.

Case	θ_a in upper 1/3 depth	θ_a in lower 2/3 depth	λ
1	< 0.2	> 0.5	0.50
2	< 0.2	0.2–0.5	0.75
3	0.2–0.5	> 0.5	0.75
4	0.2–0.5	< 0.2	1.25
5	> 0.5	0.2–0.5	1.25
6	> 0.5	< 0.2	1.50
Others			1.00

where U is a maximum dimensionless water-uptake rate, ranging from 0 to 1, as a function of soil available water fraction (Campbell and Norman 1998):

$$U = 1 - (1 + 1.3\theta_a)^{-b}, \qquad (15)$$

and b is an empirical parameter determined by soil texture, and is available in Campbell and Norman (1998).

Equation (14) reflects the relative importance of the root distribution and hence takes into account the water stress compensation.

The choice of the root water–uptake function affects the soil moisture profile because of the water stress compensation and thereby has a strong impact on runoff simulation. As a result the runoff with the new dynamic root water–uptake function is relatively lower as compared with the original function (Fig. 3).

c. Infiltration

Green and Ampt (1911) developed a theoretical equation to predict infiltration capacity based on Darcy's law. For soils that are homogeneous, deep, and well drained, infiltration rates can be expressed as (Rawls et al. 1983)

$$f = K\left(1 + \frac{H_f M_d}{I}\right), \qquad (16)$$

where f is the infiltration rate, K the hydraulic conductivity, and H_f the capillary pressure head at the wetting front; M_d is the soil moisture difference equal to ($\theta_s - \theta_i$) with θ_s being saturated soil moisture content and θ_i initial soil moisture content at the start of the rain, and I is the total infiltrated depth.

Solving Eq. (16) for the middle of the time step yields (Julien et al. 1995)

$$f^{t+\Delta t/2} = \frac{1}{2\Delta t}\Big\{[K\Delta t - 2I^t] + [(K\Delta t - 2I^t)^2$$
$$+ 8(KI^t + KH_f M_d)\Delta t]^{1/2}\Big\}, \qquad (17)$$

where t is time, and Δt is the time step.

Equation (17) is used for homogeneous soils, but in practice soils are often heterogeneous. For simplicity we assume the soil profile is homogeneous from the perspective of hydraulic conductivity and take the K value of the top soil layer as the K value of Eq. (17), while M_d and H_f are estimated based on the heterogeneous soil profiles.

The runoff simulated with Green–Ampt infiltration model is much less than with the original infiltration model (Fig. 5). This is because the Green–Ampt model allows for more water infiltration into the soils and subsequently more water is available for evapotranspira-
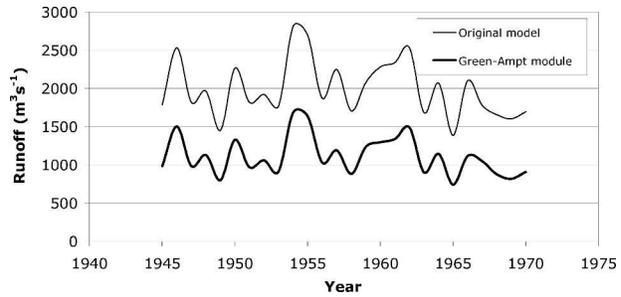

FIG. 5. Runoff simulated with original and Green–Ampt infiltration module in the LCB.

tion by the plants, compared to the original IBIS infiltration module.

d. Weather generation

From the initial simulations we found that the weather generator used in IBIS may sometimes generate unrealistically large amounts of daily rainfall. This is one of the major causes for runoff overestimation due to rapid saturation of upper soil layers and large overland flow. To prevent the weather generator from generating any unrealistically large rainfall event, we set a maximum daily rainfall; if any daily rainfall is over the prescribed maximum daily rainfall the weather generator will regenerate the daily rainfall data. As the climate may be quite different from one subbasin to another within a large basin such as NRB and LCB, the maximum daily rainfall should be a distributed parameter. We propose that the maximum daily rainfall is linearly proportional to the annual rainfall, expressed as

$$R_{\max} = \max(60, cR_a), \qquad (18)$$

where $R_{\max}$ is the maximum daily rainfall (mm), R_a the annual rainfall (mm), and c an empirical parameter being 0.08 for LCB and 0.18 for NRB, obtained through calibrations. The criterion for calibrating c is that the discrepancy should fall within such a range that further fine tuning of the maximum puddle depth is able to fit the simulated data to the observations. Instead of calibrating the $R_{\max}$ for each subbasin, the use of this function considerably reduces the amount of calibration work.

e. Runoff

As previously described, the surface runoff in IBIS is controlled by an empirical lumped parameter called maximum puddle depth. From the initial simulations we found that allowing maximum puddle depth to vary in space and time (changing with wet and dry places

and times) results in more realistic representation of the runoff in comparison to observations. Our simulations show that the puddle depth is strongly associated with the rainfall regime: the dryer the region, the larger the maximum puddle depth. Accordingly, we set the maximum puddle depth to be a function of annual rainfall:

$$D_{max} = \max(1, L - 0.0125 R_a), \qquad (19)$$

where D_{max} is the maximum puddle depth (mm) and R_a the annual rainfall (mm); L is the upper limit of the maximum puddle depth (mm), an empirical parameter being 35 for LCB and 20 for NRB, which are obtained through calibration. With this function, the maximum puddle depth varies spatially and temporally with the changes of annual rainfall and eliminates the need for calibrating individually for each subbasin.

The fact that a larger puddle depth is associated with the dry region can be explained as being primarily due to the marked degradation of drainage networks as a result of highly intermittent streamflow characteristics. The dry northern basins are characterized by the endorheic (inward draining) hydrology (Sircoulon et al. 1999); that is, many ephemeral pools are formed at the beginning of the rainy season, which dry out 2–3 months after the last rainfall. The larger puddle depth allows the excessive rainfall to eventually infiltrate into the soil or evaporate to the air without externally flowing into the river system.

4. Model calibration and validation

The model contains many empirical parameters: it is impossible to calibrate and validate all these parameters. In this study, only those most sensitive parameters that have considerable impacts on the simulation results are calibrated and validated. These empirical parameters include those in the maximum daily rainfall function [Eq. (18)] and maximum puddle depth function [Eq. (19)]. The IBIS annual mean runoff is calibrated and validated against the observed annual river discharge in both river systems. The model performance is evaluated using two indices of error statistics (Ambrose and Roesch 1982), root-mean-square error (RMSE) and relative error (RE), expressed as

$$RE = \frac{100 \sum\limits_{i=1}^{n} (S_i - M_i)}{n M_{mean}}, \qquad (20)$$

$$RMSE = 100 \left[\frac{\sum\limits_{i=1}^{n} (S_i - M_i)^2}{n} \right]^{0.5} \Big/ M_{mean}, \qquad (21)$$

TABLE 2. Relative error (RE) and rms error (RMSE) of simulated annual discharge.

Basin	Calibration/validation		RE (%)	RMSE (%)
LCB	Calibration	1937–46	3.0	18.8
	Validation	1953–64	5.9	18.5
		1965–94	18.7	31.9
	All combined	1937–94	10.7	24.3
NRB	Calibration	Gaya	4.9	12.6
	Validation	Dire	−0.5	10.5
		Niamey	9.3	18.3
		Douna	−11.1	26.4
	All combined	All stations	2.5	15.7

where M_i is the corresponding measured value and M_{mean} is the average of the measurements. RMSE (%) is an error statistic for evaluating the accuracy of the model, while RE (%) is used to check if the model systematically over or underestimates. The model calibration is targeted for a minimum square of the residuals in river discharge, with the following objective function:

$$OF = \sum_{i=1}^{n} \sum_{j=1}^{m} [M(t_i, s_j) - S(t_i, s_j, \mathbf{p})]^2, \qquad (22)$$

where $M(t_i, s_j)$ and $S(t_i, s_j, \mathbf{p})$ denote the measured and predicted river discharge, respectively, at time t_i and gauge station s_j, given the parameter vector $\mathbf{p}$.

Because data from only one discharge gauging station is available in LCB (at N'Djamena, see location in Fig. 1), validation and calibration of the model for the LCB was performed for different time periods. These different time periods correspond to different climate regimes: calibration was performed for the period 1937–46 (which is a period of moderate precipitation, a mean annual of 382 mm), and validation in a relatively wet period (1953–64, with a mean annual precipitation of 430 mm) and in a relative dry period (1965–94, with a mean annual precipitation of 345 mm) using the data of Olivry et al. (1996). Calibration and validation of the NRB was performed at different gauge stations because several were available but of very limited length: calibration to the Gaya station (see location in Fig. 1), at the lower reach of the NRB, and validation at three different gauge stations (Niamey, Dire, and Douna; Fig. 1) in the upper reaches using the data of the River Discharge Database (RivDis2.0) within the period 1937–95. The gauge measurements for both basins are provided at monthly resolution, which we have averaged to annual mean.

For LCB, in the calibration period the RE between simulated and observed annual mean runoff is 3% and RMSE is 19% (Table 2). In the wet validation period,

the model performed comparably well, with RE being 6% and RMSE being 19%. However, in the dry validation period, the RE and RMSE are, respectively, 19% and 32%, significantly higher than in the wet validation period. In fact, the model performed very well in the first two-thirds of the period (1965–83) of the dry validation, and the overestimation occurred only in the second one-third period (1984–95) (Fig. 6). This overestimation may be due primarily to some or all of the following factors: 1) long-term groundwater recharge that may be taking place since the partial amelioration of the drought in the 1990s (Sircoulon et al. 1999) and limitations of our land surface model in handling groundwater recharge; 2) removal of water from streamflow by evaporation from upstream reservoirs or irrigation (Coe and Foley 2001); and 3) model parameters may not work properly under an extremely dry climate. Generally, in arid and semiarid LCB the enhanced IBIS performed very well in predicting interannual hydrology (RMSE less than 20% and RE less than 10%) except for the extremely dry period (1984–94) after the long period of persistent drought.

In NRB, the RE and RMSE for the calibration gauge station (Gaya) is 5% and 13%, respectively (Table 2). At the validation gauge stations, the RMSE ranges from 11% to 26% and the absolute value of the RE from 1% to 11%. For all stations combined, the RMSE is only 16% and RE is only 3%. The good performance of the model for NRB is also illustrated in Fig. 7.

Generally, the IBIS land surface hydrological module performs satisfactorily, and the performance is better than or comparable to other hydrological simulations with land surface models, as is indicated in a review by Döll et al. (2003) on hydrologic model performance. For example, Oki et al. (1999) compared the discharge simulated by 11 land surface models with the observed discharge from 250 stations in 150 river basins; the simulated discharge for the Mississippi River at Vicksburg, Mississippi, for example, ranged from 24 to 130 mm yr^{-1}, while the observed value was
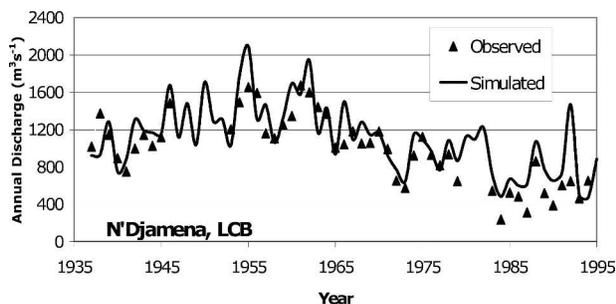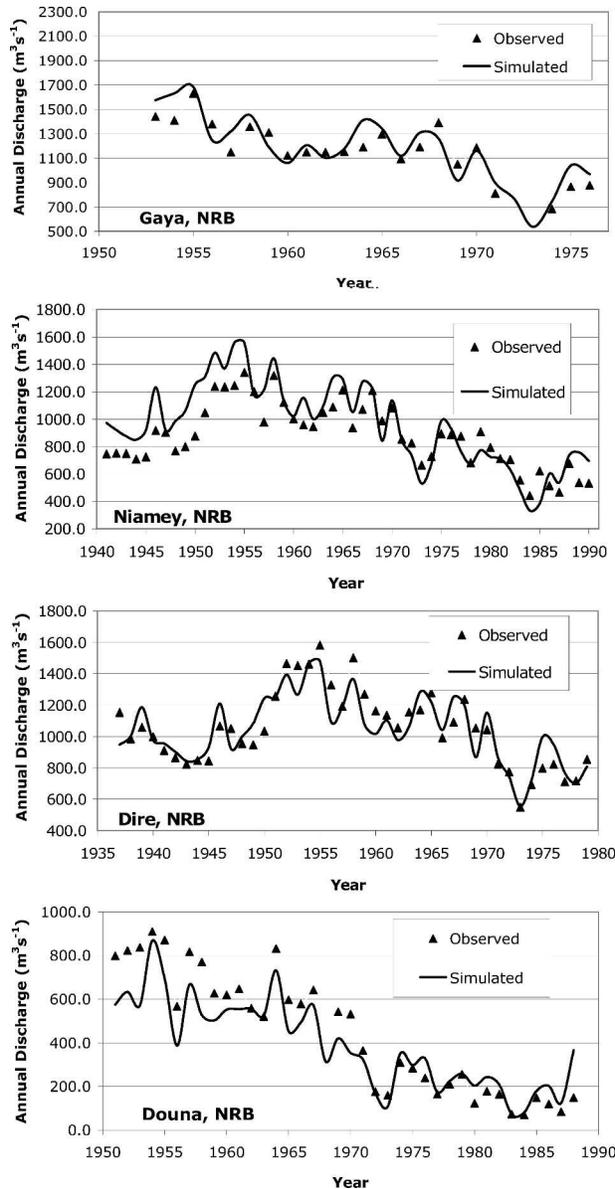

FIG. 7. Comparison of simulated and measured annual discharge at Gaya, Dire, Niamey, and Douna in the NRB.

142 mm yr^{-1}. A simulation by Meigh et al. (1999) with Macro-Probability Distributed Model (MacroPDM) of Arnell (1999a,b) showed that the simulated long-term average discharges in many large basins differed by more than 50% from the observed values. Some models consistently and systematically over- or underestimated the discharge, and hence a correction factor has to be applied to the modeled values (e.g., Fekete et al., 1999), which results in inconsistency between basin runoff/ discharge (after correction) and the evapotranspiration and soil water content. A simulation made by Nijssen et al. (2001) using the land surface model of Liang et al.

FIG. 6. Comparison of simulated and measured annual discharge at N'Djamena in the LCB.

TABLE 3. Annual rainfall (observed, mm yr^{-1}), ET, runoff (simulated, mm yr^{-1}), standard deviation (SD mm yr^{-1}), and coefficient of variance (CV, %).

	Wet period (1950–64/1969)			Dry period (1965/1970–95)			Long term (1937–95)		
	Mean	SD	CV	Mean	SD	CV	Mean	SD	CV
	Lake Chad basin								
Rainfall	432.3	32.4	7.5	343.2	41.5	12.1	373.9	53.7	14.4
ET	416.2	24.9	6.0	334.8	38.1	11.4	363.0	48.3	13.3
Runoff	15.9	3.2	20.1	9.2	2.9	31.3	11.7	4.0	34.4
Runoff coefficient	0.037			0.027			0.031		
	Niger River basin								
Rainfall	472.5	33.1	7.0	381.1	37.6	9.9	422.6	53.2	12.6
ET	425.5	25.6	6.0	353.7	29.7	8.4	386.2	42.1	10.9
Runoff	46.8	7.6	16.2	27.8	7.0	25.2	36.9	11.0	29.7
Runoff coefficient	0.099			0.073			0.087		

(1994) showed that simulated annual discharge differed from the observed value by 0.9%–22% (excluding the Senegal with 340%).

5. Temporal and spatial variability of the hydrology

The hydrological interannual variability was investigated over the period from 1950 to 1995 and was classified into contrasting wet [1950–64 (LCB)/1969 (NRB)] and dry [1965(LCB)/1970–95 (NRB)] periods. The hydrological elements for the variability analyses include observed rainfall and simulated evapotranspiration, runoff, and river discharge. The standard deviation and coefficient of variance are used to evaluate the absolute and relative temporal variability respectively. The spatial variability of precipitation, runoff, and evapotranspiration is illustrated through the maps of CV.

a. Rainfall

Rainfall fluctuation is the most prominent indicator of nature climate variation. In northern Africa, rainfall is highly variable both temporally and spatially (Nicholson 1988, 2000) and is the single most important factor affecting the hydrology and climate (Le Barbe and Lebel 1997).

The temporal variation of the rainfall in the Climatic Research Unit 2005 dataset (CRU05) during the period 1950–95 is characterized by 1) a relatively wet period from 1950 to 1964 (LCB)/1969 (NRB), with a mean annual rainfall in the simulated basin area (Fig. 1) of 432 mm for LCB and 472 mm for NRB (Table 3), which are 16% and 12% higher than the long-term mean annual rainfall respectively; 2) a persistent dry period 1965(LCB)/1970–95 (NRB), with an annual rainfall of 343 mm for LCB and 381 mm for NRB (Table 3), which

is a decrease by 8% and 10% as compared to the long-term averages. Within each single period, the interannual variability differs from the dry to the wet period: the SD and CV are higher in the dry period (42 mm and 12% for LCB and 38 mm and 10% for NRB) than in the wet period (32 mm and 8% for LCB and 33 mm and 7% for NRB; Table 3). A marked, sudden rainfall shift from wet to dry regime took place in late 1960s (Fig. 2). This sharp variation exerted major effects on the ecology, environment, and water resource management (e.g., Sarch and Birkett, 2000). The over 25-yr persistent drought, which has shifted the isohyets southward by approximately 1° of latitude (Fig. 8), has greatly reduced the river discharge rates. It is reported that the lasting drought is associated with a decrease in the number of rainy events, rather than to a decrease of the mean event rainfall (Le Barbe and Lebel 1997; Lebel et al. 1997). As expected, the long-term interannual rainfall variability, with SD being 53 mm and CV being 13%–14% for both basins (Table 3), was significantly higher than any single wet or dry period.

The rainfall varies highly with the latitude. The annual rainfall ranges from >1400 (LCB)/>1800 (NRB) mm yr^{-1} in the southern part of the basins to <200 mm yr^{-1} in the northern part (Fig. 8). The interannual variability of the rainfall is strongly associated with the latitude, with the CV ranging from 10%–15% in the south, where precipitation is relatively high, to 30%–40% in the north in both basins (Figs. 11 and 12).

b. Evapotranspiration

As with the observed rainfall, the ET simulated by IBIS increases southward for both basins from <200 in the north to >1400 mm yr^{-1} in the south. The ET is strongly linked with the rainfall, and thus shows a similar geographic variation pattern (Figs. 8, 9, 11, and 12). In LCB, the simulated ET is 416 and 335 mm yr^{-1} for
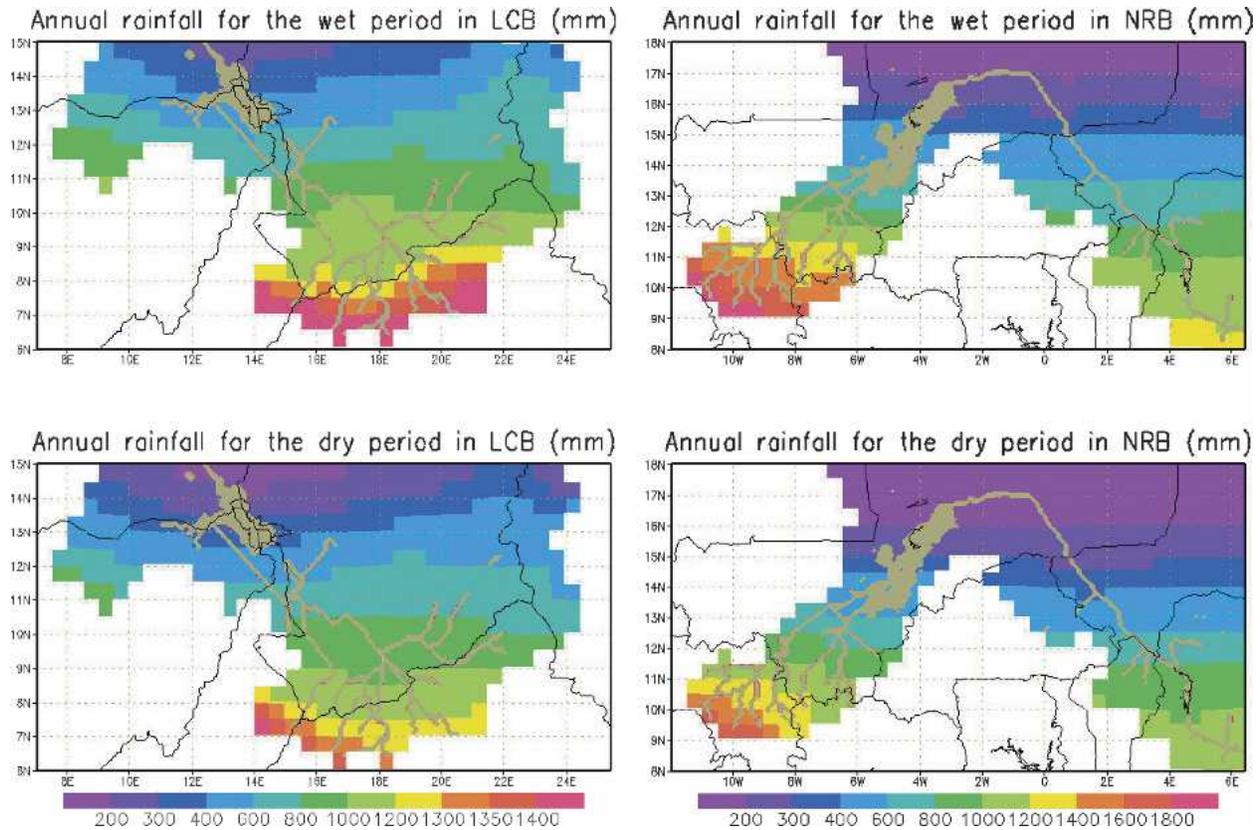
FIG. 8. Mean annual rainfall for the LCB and NRB over both wet and the dry periods.

the wet and the dry periods, respectively, which is an increase of 15% and a decrease of 8% as compared to the long-term mean (363 mm yr^{-1}; Table 3). In NRB, the ET for the wet and the dry periods is respectively 426 and 354 mm yr^{-1}, corresponding to a 10% increase and an 8% decrease in comparison with the long-term mean (386 mm). The interannual variability in terms of both SD and CV is slightly lower than the rainfall variability (Table 3; Figs. 11 and 12). Similar to rainfall variation, the interannual variability in ET is also strongly associated with the geographic location: it varies from 5%–10% in the south to 30%–40% in the north (Figs. 11 and 12).

c. Runoff

Overall, the simulated runoff is only a very small portion of rainfall in West Africa. On average (for the long-term period from 1937 to 1995), the runoff and runoff coefficient (runoff/precipitation) are respectively 12 mm yr^{-1} and 0.031 in LCB and 37 mm yr^{-1} and 0.087 in NRB (Table 3). Similar results were reported by Margat (1991), who found that arid and semi-arid zones of Africa, which account for 60% of the continent's land area, produce only about 5% of the total runoff and is illustrated by Ashton (2002), who showed that the runoff ratio in Africa is generally less than 10% when precipitation is less than 900 mm yr^{-1}. In the wet period both runoff and the runoff coefficient (16 mm yr^{-1} and 0.037 in LCB and 47 mm yr^{-1} 0.099 in NRB) are higher as compared to the long-term averages, while in the dry period they are lower (9 mm yr^{-1} and 0.027 in LCB and 28 mm yr^{-1} and 0.073 in NRB) than in the long-term period (Table 3). The relative interannual variability of runoff (CV) is over twice as high as for ET and rainfall for the long-term period and for the wet and dry periods (Table 3). The interannual variability (CV) of runoff for the long-term period (34% for LCB and 30% for NRB) is significantly larger than for any wet or dry single period although the temporal variability (CV) of the runoff is considerably higher in the dry period (31% in LCB and 25% in NRB) than in the wet period (20% in LCB and 16% in NRB; Table 3).

Additionally, the runoff is highly variable over space. The runoff varies from 300–400 mm in LCB and >400 mm in NRB in the southern part of the basins to <20 mm in the northern part (Fig. 10). The highest CVs in
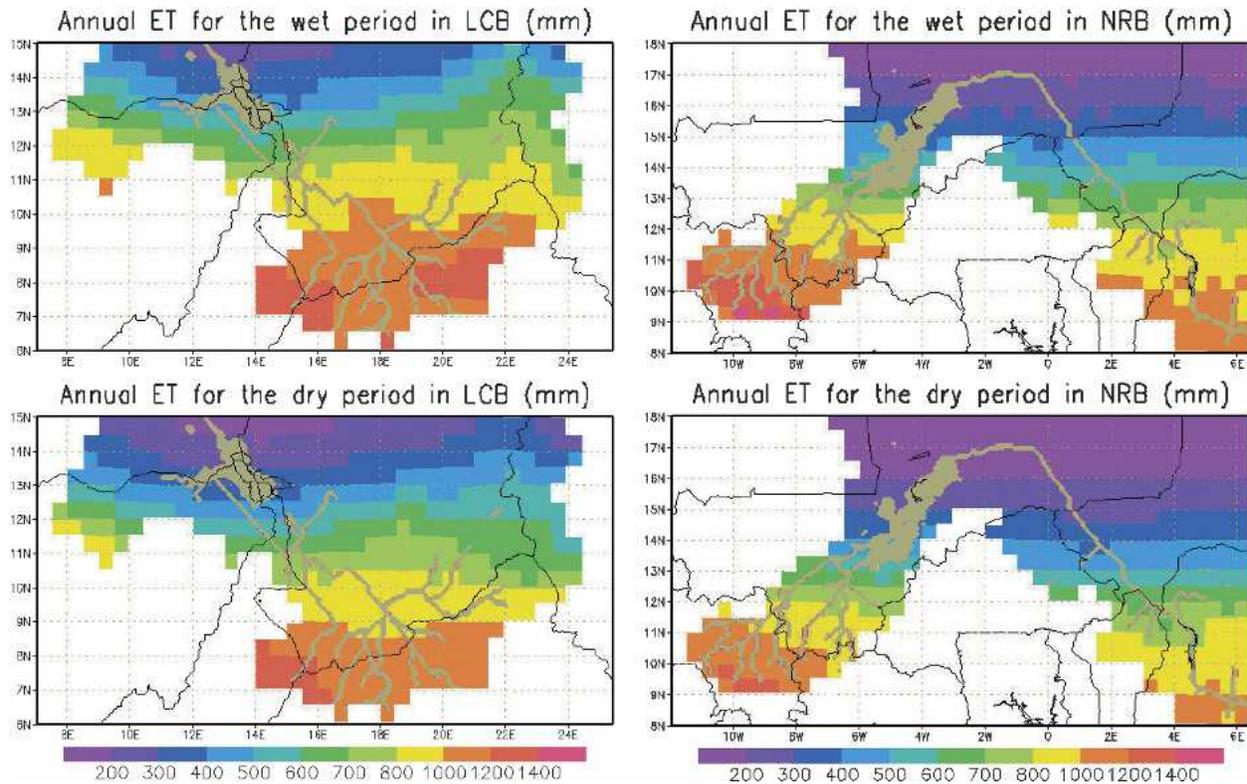
FIG. 9. Mean annual evapotranspiration (ET) for the LCB and NRB over both wet and the dry periods.

runoff (as high as 100%–200% for both basins) were found in the middle part of the basins (8°–13°N in LCB and 12°–16°N in NRB; Figs. 11 and 12). Therefore, it can be seen that the runoff and its temporal variations are very unevenly distributed in West Africa: a larger portion of the runoff is produced from southern basins; and a small portion comes from the middle portion of the basins with high interannual variability; and very little runoff is generated from the northern part of the basins.

d. River discharge

Both measurements and simulations of river discharge show similar temporal trends to the rainfall variation, and the hydrological regime shift that occurs in late 1960s is also reflected in both simulated and observed river discharge (Figs. 2, 6, and 7). In this section, we use the observed discharge to analyze the variability, but we employ the simulated values when the observed data are not available. In LCB, the observed annual river discharge at the N'Djamena gauge station is 1407 $m^3 s^{-1}$ in the wet period and 754 $m^3 s^{-1}$ in the dry period (Table 4), an increase of 43% and a decrease of 23% as compared to the long-term annual mean value (983 mm yr^{-1}). In NRB, at the Douna gauge

station in the upper basin, the relative interannual variability of the observed discharge in the wet and the dry period is 19% and 56%, respectively (the annual discharge is 698 $m^3 s^{-1}$ for the wet period and 200 $m^3 s^{-1}$ for the dry period, with a long-term annual mean of 443 $m^3 s^{-1}$). In the lower reach of NRB (Dire, Niamey, and Gaya), the discharge in the wet and dry period varies by 12%–14% in the wet period, and by 17%–25% in the dry period, significantly lower than in the upper reach due to the impact of the large wetland complex downstream of Douna that alleviates the river discharge response to the rainfall fluctuations. The discharge variability is also illustrated in the SD and CV (Table 4). For the whole period, the CV is 38% for the Chad basin, and 63% for the upper reach of NRB and 23%–31% for the lower reach, indicating that the river discharge variation is largely governed by rainfall fluctuations.

6. Conclusions

The objective of this paper was to investigate the hydrologic variability in western and central Africa using land surface models. First, the IBIS land surface hydrology module was enhanced, calibrated, and
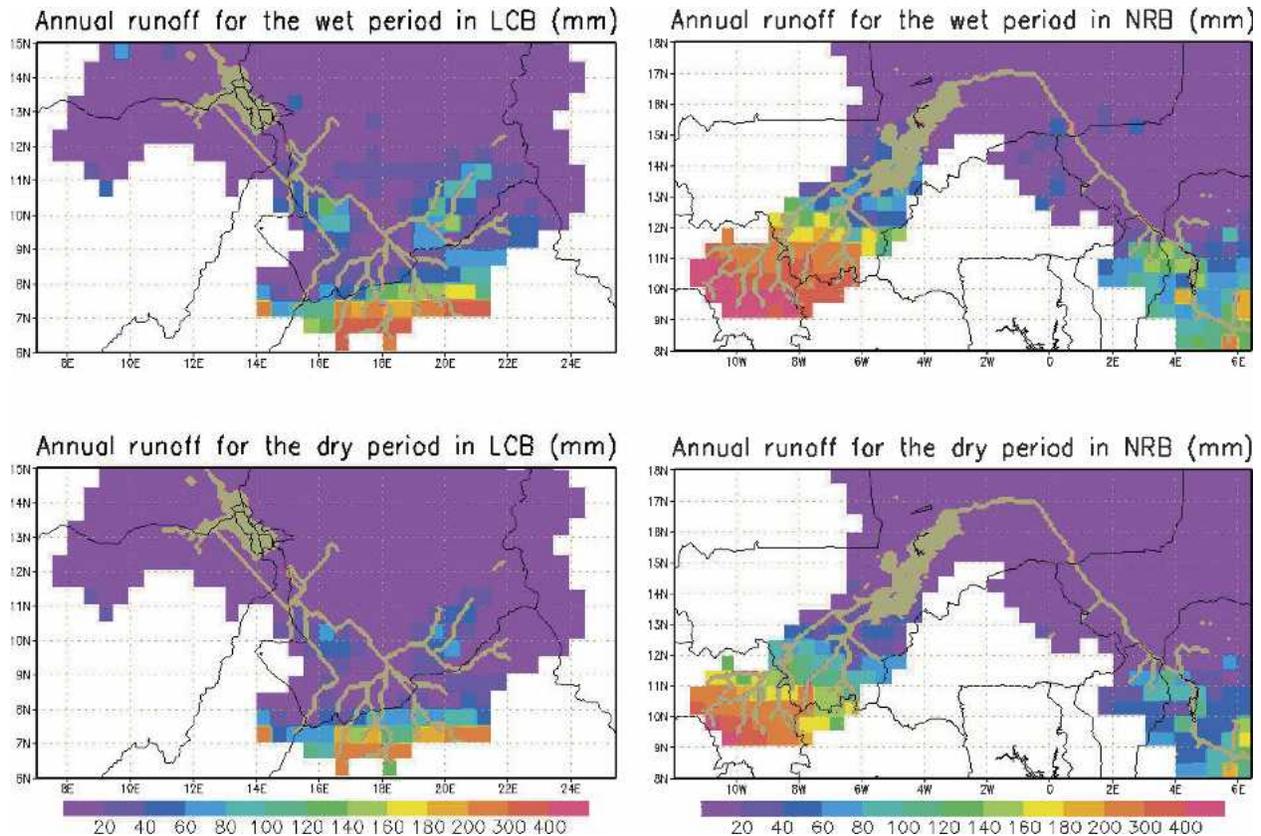
FIG. 10. Mean annual runoff for the LCB and NRB over both wet and the dry periods.

validated for West Africa. The dynamic root water–extraction module developed in this study and the incorporation of the Green–Ampt infiltration module improved the hydrological simulation in arid and semiarid Africa. The maximum puddle depth and maximum daily rainfall functions proposed in this study refined the runoff simulation and substantially reduced the need for calibration on a spatial basis. Second, with this land surface modeling approach we investigated the interannual hydrological variability including rainfall, ET, runoff, and river discharge.

The results show, in agreement with previous studies (e.g., Nicholson 2000; Nicholson and Flohn 1980) that rainfall is highly variable over both time and space, ranging from >1400 (LCB)/>1800 (NRB) mm yr^{-1} in the southern part of the basin to <200 mm yr^{-1} in the northern part, corresponding to CVs varying from 10%–15% to 30%–40% (interannual variability). The ET, with slightly lower absolute value and lower CVs, shows a rather similar geographic pattern to rainfall. The runoff and runoff coefficient are only 12 mm yr^{-1} and 0.031 in LCB and 37 mm yr^{-1} and 0.087 in NRB, indicating that the runoff is only a small portion of the rainfall. As a result, the runoff is extremely sensitive to

the rainfall fluctuation, especially in the middle portions of the basins (8°–13°N in LCB and 12°–16°N in NRB), where the CVs are as high as 100%–200%. Similar to the rainfall, the runoff is highly unevenly distributed, with the larger portion of the runoff from southern basins, a small amount from the central part and very little from the northern part of the basin. The annual river discharge highly varies with the rainfall fluctuation, with CV being 37% in LCB and 23%–63% in NRB. The hydrologic variability is significantly higher in the dry period than in the wet period, and the variability in runoff is over two times as high as in ET or rainfall.

The water resource system of LCB and NRB is very sensitive to climate variability, especially in the middle portions of the basins. The interannual climate variability in the past several decades has had considerable influence on the water resource system, and thereby on agriculture, industry, fishery, recreation, and navigation. The most spectacular example is the shrinking of Lake Chad due to the persistent drought since the late 1960s, which has largely changed the hydrologic regime and thus the economic and human activities in this region (Sarch and Birkett 2000). Water resource manage-
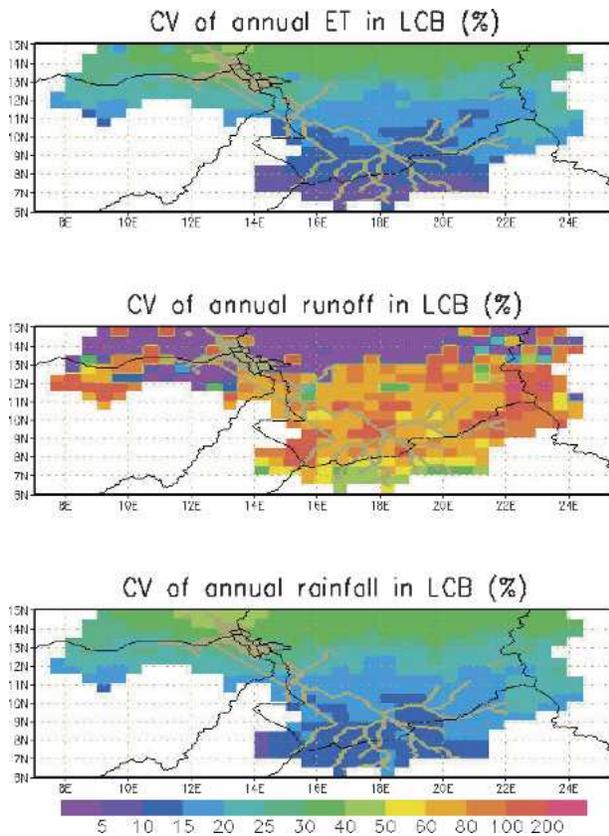
FIG. 11. Coefficient of variance (CV) of annual rainfall, ET, and runoff for the LCB over the long-term period 1950–95.
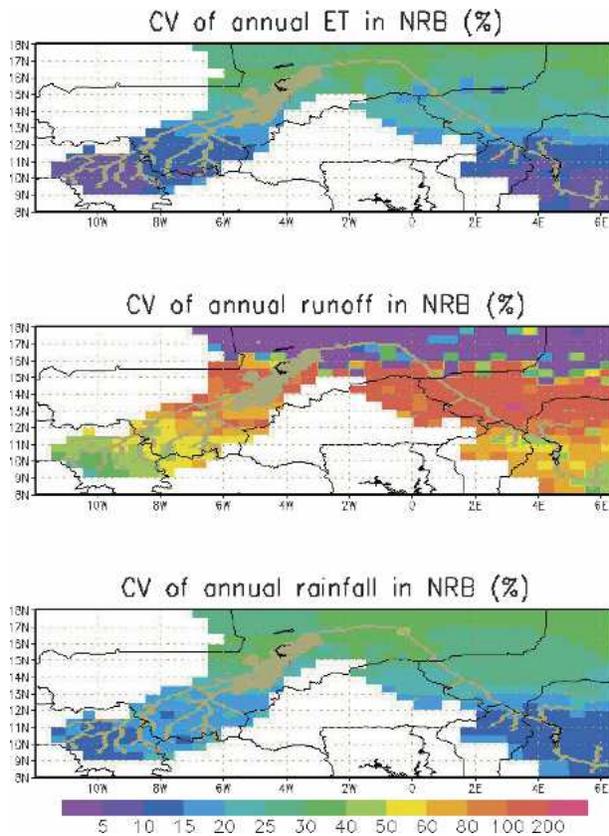

FIG. 12. Coefficeint of variance (CV of annual rainfall, ET, and runoff for NRB over the long-term period 1950–95.

ment is expected to become more challenging in the future with increasing population and potential climate changes. This study focuses on addressing the hydrologic interannual and spatial variability in response to the observed historical climate variation; further investigation is required for assessing the vulnerability and adaptability of eco-economic systems to hydrologic variability.

TABLE 4. As in Table 3, but for observed and simulated annual discharge ($m^3 s^{-1}$) at five gauge stations.

	Wet period (1950–64/1969)			Dry period (1965/1970–95)			Long term (1937–95)		
	Mean	SD	CV	Mean	std dev	CV	Mean	SD	CV
N'Djamena, LCB									
Observed	1407.0	198.7	14.1	753.6	276.8	36.7	983.1	369.1	37.5
Simulated	1497.7	313.5	21.2	918.3	278.1	30.3	1111.5	363.6	32.7
Douna, NRB									
Observed	698.0	130.8	18.7	200.4	113.1	56.4	442.5	279.3	63.1
Simulated	563.8	126.2	22.4	249.3	109.5	43.9	396.8	179.9	45.3
Dire, NRB									
Observed	1243.8	172.4	13.9	779.3	128.6	16.5	1050.6	240.2	22.9
Simulated	1192.6	163.0	13.7	723.7	181.0	25.0	940.4	262.6	27.9
Niamey, NRB									
Observed	1103.0	138.5	12.6	711.9	169.8	23.9	881.5	232.8	26.4
Simulated	1238.2	189.0	15.3	703.9	185.8	26.4	948.7	292.4	30.8
Gaya, NRB									
Observed	1261.7	155.0	12.3						
Simulated	1316.8	203.2	15.4	739.6	187.6	25.4	1002.4	312.9	31.2

REFERENCES

Ambrose, R. B., Jr., and S. E. Roesch, 1982: Dynamic estuary model performance. *J. Environ. Eng. Div. ASCE,* **108,** 51–57.

Arnell, N. W., 1999a: A simple water balance model for the simulation of streamflow over a large geographic domain. *J. Hydrol.,* **217,** 314–335.

——, 1999b: Climate change and global water resources. *Global Environ. Change,* **9,** S31–S49.

Ashton, P. J., 2002: Avoiding conflicts over Africa's water resources. *Ambio,* **31,** 236–242.

Bennie, A. T. P., 1986: The profile water supply rate: An infield evaluation with wheat. *Trans. XIII, Congress Int. Soc. Soil Sci.,* Hamburg, Germany, International Society of Soil Science, 10–11.

Campbell, G. S., and J. M. Norman, 1998: *An Introduction to Environmental Biophysics.* Springer-Verlag, 286 pp.

Canadell, J., R. B. Jackson, J. R. Ehleringer, H. A. Mooney, O. E. Sala, and E.-D. Schulze, 1996: Maximum rooting depth of vegetation types at the global scale. *Oecologia,* **108,** 583–595.

Coe, M. T., 1998: A linked global model of terrestrial hydrologic processes: Simulation of modern rivers, lakes, and wetlands. *J. Geophys. Res.,* **103,** 8885–8899.

——, 2000: Modeling terrestrial hydrologic system at the continental scale: Testing the accuracy of an atmospheric GCM. *J. Climate,* **13,** 686–704.

——, and J. A. Foley, 2001: Human and natural impacts on the water resources of the Lake Chad basin. *J. Geophys. Res.,* **106,** 3349–3356.

——, M. H. Costa, A. Botta, and C. M. Birkett, 2002: Long-term simulations of discharge and floods in the Amazon basin. *J. Geophys. Res.,* **107,** 8044, doi:10.1029/2001JD000740.

Cooper, P. J. M., P. J. Gregory, J. D. H. Keatinge, and S. C. Brown, 1987: Effects of fertilizer, variety and location on barley production under rainfed conditions in northern Syria. 2. Soil water dynamics and crop water use. *Field Crops Res.,* **16,** 67–84.

Delire, C., and J. A. Foley, 1999: Evaluating the performance of a land surface/ecosystem model with biophysical measurements from contrasting environments. *J. Geophys. Res.,* **104,** 16 895–16 909.

De Smedt, F., S. Al Khafaf, and P. J. Wierenga, 1981: Simulation of water flow in plants and soils. *Progress in Ecological Engineering and Management by Mathematical Modeling,* D. M. Dubois, Ed., Editions Cebedoc, 849–863.

Döll, P., F. Kaspar, and B. Lehner, 2003: A global hydrological model for deriving water availability indicators: Model tuning and validation. *J. Hydrol.,* **270,** 105–134.

Ehlers, W., A. P. Hamblin, D. Tennant, and R. R. van der Ploeg, 1991: Root system parameters determining water uptake of field crops. *Irrig. Sci.,* **12,** 115–124.

Fekete, B. M., C. J. Vörösmarty, and W. Grabs, 1999: Global composite runoff fields of observed river discharge and simulated water balances. Global Runoff Data Centre, Koblenz, Germany, Rep. 22, 100 pp.

Foley, J. A., I. C. Prentice, N. Ramankutty, S. Levis, D. Pollard, S. Sitch, and A. Haxeltine, 1996: An integrated biosphere model of land surface processes, terrestrial carbon balance, and vegetation dynamics. *Global Biogeochem. Cycles,* **10,** 603–628.

Gale, M. R., and D. F. Grigal, 1987: Vertical root distributions of northern tree species in relation to successional status. *Can. J. For. Res.,* **17,** 829–834.

Gardner, W. R., 1983: Soil properties and efficient water use: An overview. *Limitations to Efficient Water Use in Crop Production,* H. M. Taylor, W. R. Jordan, and T. R. Sinclair, Eds., American Society of Agronomy, 45–46.

Geng, S., F. W. T. Penning De Vries, and I. Supit, 1985: A simple method for generating daily rainfall data. *Agric. For. Meteor.,* **36,** 363–376.

Gleick, P. H., 2000: The world's water 2000–2001. *The Biennial Report on Freshwater Resources*, Island Press, 19–38.

Green, W. H., and G. A. Ampt, 1911: Studies on soil physics, 1. The flow of air and water through soils. *J. Agric. Sci.,* **4,** 1–24.

Hanan, N. P., and S. D. Prince, 1997: Stomatal conductance of west-central supersite vegetation in HAPEX-Sahel: Measurements and empirical models. *J. Hydrol.,* **188–189,** 536–562.

Hsiao, T. C., E. Fereres, E. Acevedo, and D. W. Henderson, 1976: Water stress and dynamics of growth and yield of crop plants. *Water and Plant Life,* O. L. Lange, L. Kappen, and E.-D. Schulze, Eds., Ecological Studies, Vol. 19, Springer, 281–305.

IGBP–DIS, 1999: Global soil data task: Spatial database of soil properties. International Geosphere-Biosphere Programme–Data and Information System, Toulouse, France.

Jackson, R. B., J. Canadell, J. R. Ehleringer, H. A. Mooney, O. E. Sala, and E. D. Schulze, 1996: A global analysis of root distributions for terrestrial biomes. *Oecologia,* **108,** 389–411.

——, H. A. Mooney, and E. D. Schulze, 1997: A global budget for fine root biomass, surface area, and nutrient contents. *Ecology,* **94,** 7362–7366.

Julien, P. Y., B. Saghafian, and F. L. Ogden, 1995: Raster-based hydrologic modeling of spatially-varied surface runoff. *Water Resour. Bull.,* **31,** 523–536.

Kucharik, C. J., J. A. Foley, C. Delire, V. A. Fisher, M. T. Coe, J. D. Lenters, C. Young-Molling, and N. Ramankutty, 2000: Testing the performance of a dynamic global ecosystem model: Water balance, carbon balance, and vegetation structure. *Global Biogeochem. Cycles,* **14,** 795–825.

Leavesley, G. H., 1994: Modeling the effects of climate change on water resources—A review. *Climate Change,* **28,** 159–177.

Le Barbe, L., and T. Lebel, 1997: Rainfall climatology of HAPEX-Sahel region during the years 1950–1990. *J. Hydrol.,* **188–189,** 43–73.

Lebel, T., J. D. Taupin, and N. D'Amato, 1997: Rainfall monitoring during HAPEX-Sahel. 1. General rainfall conditions and climatology. *J. Hydrol.,* **188–189,** 74–96.

Legesse, D., C. Vallet-Coulomb, and F. Gasse, 2003: Hydrological response of a catchment to climate and land use changes in Tropical Africa: Case study South Central Ethiopia. *J. Hydrol.,* **275,** 67–85.

Lenters, J. D., M. T. Coe, and J. A. Foley, 2000: Surface water balance of the continental United States, 1963–1995: Regional evaluation of a terrestrial biosphere model and NCEP/NCAR reanalysis. *J. Geophys. Res.,* **105,** 22 393–22 425.

Li, K. Y., R. De Jong, and J. B. Boisvert, 2001: An exponential

root-water-uptake model with water stress compensation. *J. Hydrol.,* **252,** 189–204.

Liang, X., D. P. Lettenmaier, E. F. Wood, and S. J. Burges, 1994: A simple hydrologically based model of land surface water and energy fluxes for general circulation models. *J. Geophys. Res.,* **99** (D3), 14 415–14 428.

Margat, J., 1991: Ressources en eau des pays Africains: Utilisation et problèmes. *7è Congrès Mondial des Ressources en Eaux,* Rabat, Morocco, IWRA/AIRE, 554-27–554-47.

Meigh, J. R., A. A. McKenzie, and K. J. Sene, 1999: A grid-based approach to water scarcity estimates for Eastern and Southern Africa. *Water Resour. Manage.,* **13,** 85–115.

New, M., M. Hulme, and P. D. Jones, 2000: Representing twentieth-century space–time climate variability. Part II: Development of 1901–96 monthly terrestrial climate fields. *J. Climate,* **13,** 2217–2238.

Nicholson, S. E., 1988: Land surface–atmosphere interaction: Physical processes and surface changes and their impacts. *Prog. Phys. Geogr.,* **12,** 36–65.

——, 2000: Land surface processes and Sahel climate. *Rev. Geophys.,* **38,** 117–139.

——, and H. Flohn, 1980: African environmental and climatic changes and the general atmospheric circulation in late pleistocene and holocene. *Climate Change,* **2,** 313–348.

Nijssen, B., G. M. O'Donnell, D. P. Lettenmaier, D. Lohmann, and E. F. Wood, 2001: Predicting the discharge of global rivers. *J. Climate,* **14,** 3307–3323.

Oki, T., T. Nishimura, and P. Dirmeyer, 1999: Assessment of annual runoff from land surface models using Total Runoff Integrating Pathways (TRIP). *J. Meteor. Soc. Japan,* **77,** 235–255.

Olivry, J.-C., A. Chouret, G. Vuillaume, J. Lemoalle, and J.-P. Bricquet, 1996: Hydrologie du Lac Tchad. *ORSTOM, Monogr. Hydrol.,* Vol. 12, ORSTOM, 266 pp.

Passioura, J. B., 1985: Roots and water economy of wheat. *Wheat Growth and Modelling*, W. Day and R. K. Atkin, Eds., Plenum Press, 185–198.

Pollard, D., and S. L. Thompson, 1995: Use of a land-surface-transfer scheme (LSX) in a global climate model: The response to doubling stomatal resistance. *Global Planet. Change,* **10,** 129–161.

Ramankutty, N., and J. A. Foley, 1999: Estimating historical changes in global land cover: Croplands from 1700 to 1992. *Global Biogeochem. Cycles,* **13,** 997–1027.

Rawls, W. J., D. L. Brakensiek, and N. Miller, 1983: Green–Ampt infiltration parameters from soils data. *J. Hydraul. Eng. ASCE,* **109,** 62–70.

Richardson, C. W., 1981: Stochastic simulation of daily precipitation, temperature, and solar radiation. *Water Resour. Res.,* **17,** 182–190.

——, and D. A. Wright, 1984: WGEN: A model for generating daily weather variables. U.S. Dept. of Agriculture, Agriculture Research Service ARS-8, Washington, D.C., 83 pp.

Sarch, M. T., and C. Birkett, 2000: Fishing and farming at Lake Chad: Response to lake-level fluctuations. *Geophys. J.,* **166,** 156–172.

Sircoulon, J., T. Lebel, and N. W. Arnell, 1999: Assessment of the impacts of climate variability and change on the hydrology of Africa. *Impacts of Climate Change and Climate Variability on Hydrological Regimes,* J. C. Van Dam, Ed., Cambridge University Press, 67–84.

Taylor, H. M., and B. Klepper, 1975: Water uptake by cotton root systems: An examination of assumptions in the single root model. *Soil Sci.,* **120,** 57–67.

Thompson, S. L., and D. Pollard, 1995a: A global climate model (GENESIS) with a land-surface-transfer scheme (LSX). Part I: Present-day climate. *J. Climate,* **8,** 732–761.

——, and ——, 1995b: A global climate model (GENESIS) with a land-surface-transfer scheme (LSX). Part II: CO_2 sensitivity. *J. Climate,* **8,** 1104–1121.

van der Ploeg, R. R., F. Beese, O. Strebel, and M. Renger, 1978: The water balance of a sugar beet crop: A model and some experimental evidence. *Z. Pflanzenern. Bodenk.,* **141,** 313–328.

Williams, J. R., 1995: The EPIC model. *Computer Models of Watershed Hydrology*, V. P. Singh, Ed., Water Resources Publications, 909–1000.